2023 IEEE International Conference on Robotics and Automation (ICRA 2023)
May 29 - June 2, 2023. London, UK

An equivalent two section method for calculating the workspace of multi-segment continuum robots

Yeman Fan, *Student Member, IEEE*, and Dikai Liu, *Senior Member, IEEE*

***Abstract*—Obtaining the shape and size of a robot's workspace is essential for both its design and control. However, determining the accurate workspace of a multi-segment continuum robot by graphic or analytical methods is a challenging task due to its inherent flexibility and complex structure. Existing numerical methods have limitations when applied to a continuum robot. This paper presents an Equivalent Two Section (ETS) method for calculating the workspace of multi-segment continuum robots. This method is based on the forward kinematics and a piecewise constant curvature (PCC) model to determine the boundaries of the workspace. In order to verify the proposed method, simulation experiments are conducted using six different maximum bending angles and seven different number of segments. Results of the ETS method are compared to the true workspaces of these configurations estimated by an exhaustive approach. The results show that the proposed ETS method is both efficient and accurate, and has small estimation errors. Discussions on the advantages and limitations of the proposed ETS method are also presented.**

I. INTRODUCTION

Continuum robots have many advantages when compared to traditional rigid robots, including inherent compliance, flexibility, and dexterity [1]. This type of robot has immense potential to be applied in various applications, such as medical services [2], non-destructive inspections [3], and grasping tasks [4]. Recently, many diffident continuum robots have been designed. Examples include flexible manipulators designed for minimally invasive surgery [5]-[7] and MRI-guided neurosurgery [8], an omnidirectional-steering continuum manipulator [9], cable-driven snake-like manipulators [10]-[12], and other general variable stiffness continuum robots [13]-[18]. To the best of our knowledge, there is no efficient method in the literature for calculating the workspace of a continuum robot with a high number of segments. However, obtaining a robot's workspace, in terms of shape and size, is essential for robot design, control and planning [19] [20].

The workspace of a robot is defined as the set of positions that can be reached by its distal point, which is an important kinematic factor in measuring a robot's workability. Generally, workspace calculation methods can be categorized into three types: graphic methods, analytical methods [21] [22], and numerical methods [23]-[26]. Analytical methods use multiple envelopes to determine the boundary of the workspace, which results in efficient calculation and high precision but with poor versatility and practicability [25]. Numerical methods calculate the distal point positions based on extreme value theory, brute-force enumeration, or optimization methods. They generate a workspace by calculating the feature points on the boundary of the workspace. A commonly used numerical method is the Monte Carlo method which uses the means of random sampling and is relatively simple to apply because it does not need inverse Jacobian calculation [24].

The brute-force Monte Carlo method needs sufficient sampling points to achieve reasonable precision, which has the shortcoming of low efficiency and large calculation errors [27]. A relatively more accurate workspace was calculated by combining the Beta distribution with the Monte Carlo method [23] [24]. By using the Gaussian growth method, an improved Monte Carlo method was proposed to attain higher workspace accuracy [27]. In [25], a Monte Carlo learning method based on boundary point densification was proposed. Although these methods improved the classical Monte Carlo method by taking advantage of the Beta distribution or Gaussian growth method to increase the density of boundary points, they need sufficient sampling points to obtain reasonable precision, which still has a high computational cost.

When the classical or improved Monte Carlo methods are applied to calculate the workspace of a multi-segment continuum robot, we found that most of the sample points overlap and are located in the high-probability regions of the workspace, which was also found by other researchers [23] [24] [27]. This makes it difficult to characterize the true shape and size of the workspace of a continuum robot. When a continuum robot has a high number of segments, these methods may not be able to find the complete workspace. In order to overcome this problem, we propose an Equivalent Two Section (ETS) method to calculate the workspace for continuum robots with a high number of segments. The ETS method can represent the multi-segment continuum robot with an equivalent two sections robot, and then utilizes forward kinematics and a piecewise constant curvature (PCC) model to generate the workspace boundary for calculating its workspace area and volume. And to verify the proposed ETS method, simulation experiments are conducted using six different maximum bending angles and seven different number of segments. The true workspaces of these configurations are estimated by an exhaustive approach, and the results of the ETS method are compared to these estimates for validation. The main contributions of this work include:

i) An Equivalent Two Section (ETS) method for calculating workspace area and volume of multi-segment continuum robots.

ii) Extensive verification of the proposed ETS method.

This work was supported in part by the Australian Research Council (ARC) Discovery Project Grant [DP200102497], and the Robotics Institute at the University of Technology Sydney, Australia. *(Corresponding authors: Yeman Fan)*

Yeman Fan and Dikai Liu are with the Robotics Institute, University of Technology Sydney, Sydney, NSW 2007, Australia (e-mail: yeman.fan@student.uts.edu.au; dikai.liu@uts.edu.au).

The rest of this paper is organized as follows. Section II presents the proposed ETS method. Section III describes the simulation experiments and results. Section IV presents the discussions of the method, including its advantages and limitations. The conclusion is presented in Section V.

II. Equivalent Two Section (ETS) Method

A. Common structure and parameters of continuum robots

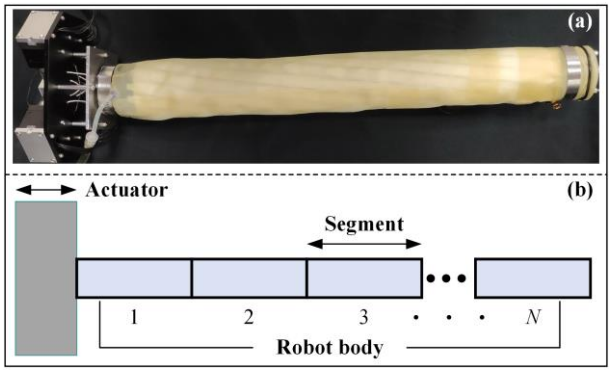

Fig. 1. (a) Photo of an example tendon-actuated continuum robot [18]. (b) A diagram of general continuum robots.

As shown in Fig. 1, a continuum robot generally consists of an actuator and a flexible robot body. The robot body normally has many segments and each with bending capability. According to the existing prototypes (Table I), three common primary parameters of continuum robots are identified: the length of each segment, the number of segments, and the maximum bending angle of a segment. Apparently, the workspace size and shape of a continuum robot are mainly determined by these three parameters. Generally, all the segments are identical in a continuum robot, therefore, an assumption made for this research is that a continuum robot consists of many segments, and all the segments have the same length and maximum bending angle.

TABLE I
Summary of Parameters of Existing Continuum Robots

No.	Robot length (mm)	Number of segments	Bending angle (°)	Ref.
1	550 165	10 (Body) 10 (Tip)	−10 ~ +90 −90 ~ +90	[3]
2	40	4	±60	[6]
3	65	3	45	[8]
4	30	2	N/A	[9]
5	4200	12	±60	[10]
6	1500 2300	6 10	20 20	[11]
7	60	6	±90	[12]
8	630	3	60	[13]
9	210	3	36	[14]
10	831	3	90	[15]
11	560	4	±45	[16]
12	165	3	83	[17]
13	504	2	180	[18]

B. Kinematic model

For calculating the distal position of a continuum robot, the PCC model is helpful for kinematic calculation [29]-[31]. This model is based on the constant curvature assumption to assume that each segment has a constant curvature (can change with different bending conditions). Fig. 2 shows the geometric relationship of a multi-segment continuum robot based on the PCC model and an example constant curvature segment.

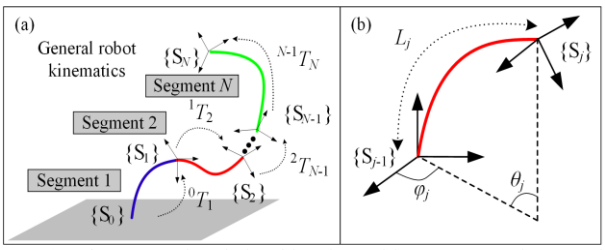

Fig. 2. (a) The geometric relationship of a multi-segment continuum robot. (b) An example constant curvature segment.

Based on the PCC model, the distal position can be calculated according to the general robot kinematics. As shown in Fig. 2(b), the curvature of a segment is determined by the segment length (L_j), bending angle (θ_j), and rotation angle (φ_j). Once the segment length is determined, according to the geometric relationship, the coordinate of a point on a continuum robot depends on the bending angle (θ_j), rotation angle (φ_j) and the reference coordinate system, which can be formulated by a 4×4 homogeneous transformation matrix

$$ {}^{j-1}\boldsymbol{T}_j = \begin{bmatrix} R_j & P_j \\ 0 & 1 \end{bmatrix} \tag{1} $$

$$ R_j = \begin{bmatrix} \mathrm{c}^2\varphi_j\mathrm{c}\theta_j + \mathrm{s}^2\varphi_j & \mathrm{c}\varphi_j\mathrm{s}\varphi_j\mathrm{c}\theta_j - \mathrm{c}\varphi_j\mathrm{s}\varphi_j & \mathrm{c}\varphi_j\mathrm{s}\theta_j \\ \mathrm{c}\varphi_j\mathrm{s}\varphi_j\mathrm{c}\theta_j - \mathrm{c}\varphi_j\mathrm{s}\varphi_j & \mathrm{s}^2\varphi_j\mathrm{c}\theta_j + \mathrm{c}^2\varphi_j & \mathrm{s}\varphi_j\mathrm{s}\theta_j \\ -\mathrm{c}\varphi_j\mathrm{s}\theta_j & -\mathrm{s}\varphi_j\mathrm{s}\theta_j & \mathrm{c}\theta_j \end{bmatrix} \tag{2} $$

$$ P_j = \begin{bmatrix} \frac{L_j}{\theta_j}\mathrm{c}\varphi_j(1-\mathrm{c}\theta_j) & \frac{L_j}{\theta_j}\mathrm{s}\varphi_j(1-\mathrm{c}\theta_j) & \frac{L_j}{\theta_j}\mathrm{s}\theta_j \end{bmatrix}^T \tag{3} $$

where j is the segment number. $\mathrm{s}\theta_j = \sin\theta_j$, $\mathrm{c}\theta_j = \cos\theta_j$, $\mathrm{s}\varphi_j = \sin\varphi_j$, $\mathrm{c}\varphi_j = \cos\varphi_j$, $\mathrm{s}^2\varphi_j = (\sin\varphi_j)^2$, $\mathrm{c}^2\varphi_j = (\cos\varphi_j)^2$, $\varphi_j \in [0, 2\pi]$.

From (3), there is a singularity at $\theta_j = 0$. Therefore, in this research, $\theta_{min} = 0.0001$ is used to replace the singular point ($\theta_j = 0$) in all the calculations. From kinematics, the coordinate system $\{S_N\}$ relative to the base coordinate system $\{S_0\}$ can be expressed as

$$ {}^0\boldsymbol{T}_N = {}^0\boldsymbol{T}_1\,{}^1\boldsymbol{T}_N \cdots {}^{N-1}\boldsymbol{T}_N = \begin{bmatrix} n_x & o_x & a_x & p_x \\ n_y & o_y & a_y & p_y \\ n_z & o_z & a_z & p_z \\ 0 & 0 & 0 & 1 \end{bmatrix} \tag{4} $$

C. True workspace estimation

From (4), all the feasible positions of the robot distal point can be calculated, and the true workspace can be obtained if the sample configurations are sufficient. As discussed in Section I, the true workspace of a continuum robot with a high number of segments is hard to obtain. Therefore, an exhaustive approach is used to estimate the workspace, which is considered as the approximation of the true workspace. **Algorithm 1** presents the exhaustive approach to estimating the workspace area (A) or volume (V) of a continuum robot by

exhaustively generating the configurations of each segment. For simplicity, the term "true workspace" used in this paper means the workspace estimated by using the exhaustive approach. This workspace will be used to analyze the accuracy and efficiency of the proposed ETS method.

Algorithm 1: Workspace calculation by an exhaustive approach

Inputs: Sampling interval value D; Number of segments N; Maximum bending angle θ_{max}; Section length L;
Outputs: Workspace area (A) and volume (V)
Algorithm:
  for $i \leftarrow 1$ to N **do**
    $\boldsymbol{\theta}_i \leftarrow [\theta_{min}, D, 2D, \ldots, \theta_{max}]$
    $\boldsymbol{\theta}_i \leftarrow [\boldsymbol{\theta}_i*\cos(0), \boldsymbol{\theta}_i*\cos(\pi)]$ ▷Generate the bending angle matrix
  end for
  $J \leftarrow (2\theta_{max}/D+2)\text{^}N$ ▷Calculate sample size
  for $j \leftarrow 1$ to J **do**
    $[{}^0\boldsymbol{T}_1, {}^1\boldsymbol{T}_2, \ldots, {}^{N-1}\boldsymbol{T}_N] \leftarrow f\{\boldsymbol{\theta}_i, L, j\}$ ▷Calculate the HTM, Eq.(1)
    ${}^0\boldsymbol{T}_N \leftarrow {}^0\boldsymbol{T}_1 * {}^1\boldsymbol{T}_2 \ldots * {}^{N-1}\boldsymbol{T}_N$
    $\boldsymbol{P}[x, z] \leftarrow f\{{}^0\boldsymbol{T}_N\}$ ▷Calculate the distal position matrix, Eq.(4)
  end for
  [BL, A] ← *find the boundary line* (BL) *and area* (A) *of* $\boldsymbol{P}[x, z]$
  BS ← *rotate* BL *to generate the boundary surface* (BS)
  V ← *calculate the volume of* BS
  return A, V

The exhaustive approach can only estimate the true workspace of a continuum robot with a small number of segments and intervals. With the increase of the number of segments, the sample configurations of the distal positions will increase exponentially. For example, if the number of segments is N=10, the maximum bending angle θ_{max}=180° and the sampling interval D=2°, the total number of total distal point positions to be calculated will be 181^{10}. The computational cost can be reduced by increasing the interval angle. For example, when the sampling interval is increased to D=180°, the total number of distal positions to be calculated will decrease to 3^{10}. However, this large sampling interval will result in sparse distal point positions, and incomplete and inaccurate workspace.

D. The equivalent two section method

In order to calculate the workspace of a continuum robot with a high number of segments, the ETS method is proposed. When the maximum bending angle (θ_{max}) and the number of segments (N) are determined, the robot model can be replaced by the ETS robot model for estimating its workspace, as shown in Fig. 3. The ETS method utilizes the Equivalent Section 1 to represent the first several segments and the Equivalent Section 2 to replace the remaining segments. In order to realize high accuracy, the Equivalent Section 1 should have enough maximum bending angle to reach all the feasible workspace boundaries. Therefore, the parameters of the ETS robot model can be derived as

$$L_{E1} = \begin{cases} L & (\theta_{max} \geq \pi) \\ \pi L / \theta_{max} & (\theta_{max} < \pi) \end{cases} \quad (5)$$

$$L_{E2} = NL - L_{E1} \quad (6)$$

$$\theta_{E1max} = \begin{cases} \pi & (\theta_{max} \geq \pi) \vee (\pi / \theta_{max} \leq N-1) \\ (N-1)\theta_{max} & (\pi / \theta_{max} > N-1) \end{cases} \quad (7)$$

$$\theta_{E2max} = \begin{cases} \pi & (\theta_{max} \geq \pi) \vee (N\theta_{max} - \theta_{E1max} \geq \pi) \\ N\theta_{max} - \theta_{E1max} & (N\theta_{max} - \theta_{E1max} < \pi) \end{cases} \quad (8)$$

Where L is the segment length of a continuum robot, L_{E1} is the length of the first equivalent section of the ETS robot model, L_{E2} is the second equivalent section length, θ_{E1max} is the maximum bending angle of the first equivalent section of the ETS robot model, θ_{E2max} is the maximum bending angle of the second equivalent section.

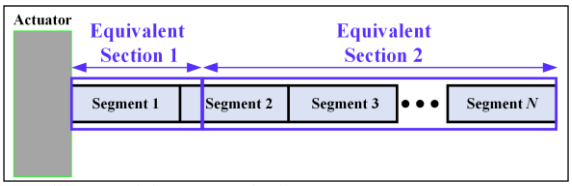

Fig. 3. A diagram of the ETS method.

As shown in Fig. 3, the multi-segment continuum robot can now be represented with an equivalent two section robot according to the ETS method. For example, when the robot parameters are N=3, θ_{max}=180°, and L=50mm, the parameters of the ETS model are θ_{E1max}=θ_{E2max}=180°, L_{E1}=50mm, and L_{E2}=100mm; when the robot parameters are N=8, θ_{max}=120°, and L=50mm, the parameters of the ETS model are θ_{E1max}=θ_{E2max}=180°, L_{E1}=75mm, and L_{E2}=325mm.

Once the parameters θ_{E1max}, θ_{E2max}, L_{E1} and L_{E2} are obtained, the ETS robot model can be used to calculate the workspace of a continuum robot. In order to demonstrate and verify the proposed ETS method, an example overlap 2D workspace is shown in Fig. 4. The true workspace area [Green] is estimated by the exhaustive approach (**Algorithm 1**), and the workspace area calculated by the ETS method is the area covered by the boundary lines [Blue].

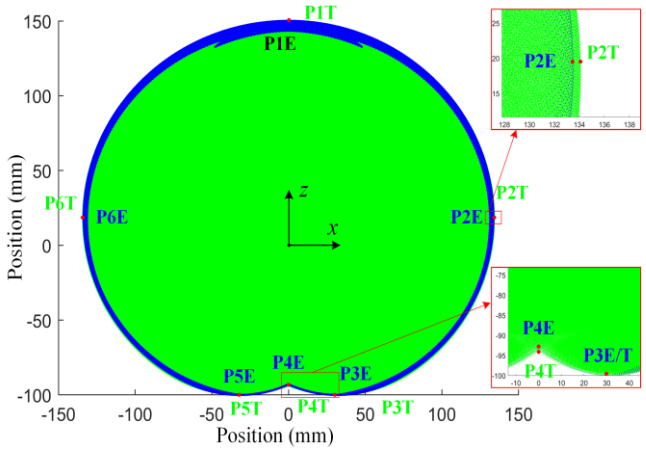

Fig. 4. An example 2D workspace and boundary features of a continuum robot with N=3, L=50mm, θ_{max}=180°. The green color shows the true workspace area, and the blue color shows the boundary generated by the ETS method.

The points P1T-P6T and P1E-P6E in Fig. 4 are feature points of the true workspace and the boundary lines calculated by the ETS method, respectively. P1T and P1E are the points with maximum z position value on the true workspace and the boundary from the ETS method, respectively. P2T and P2E, and P6T and P6E are the points with maximum and minimum x position values on the true workspace and the boundary of the ETS method, respectively. P3T and P3E and P5T and P5E are the points with minimum z value on the true workspace and the boundary of the ETS method, respectively. P4T and P4E are the points with x= 0 on the true workspace and the

boundary of the ETS method, respectively. We found that P1T and P1E always overlap, and P2T and P6T, P2E and P6E, P3T and P4T, and P3E and P4E are symmetry about the z-axis, respectively. Their values can be calculated from (9).

$$\begin{cases} x_{\mathrm{P1T}} = p_x\big|_{\theta_{i=1,\ldots,N}=\theta_{\min},\ \varphi_{i=1,\ldots,N}=0} \approx 0 \\ z_{\mathrm{P1T}} = p_z\big|_{\theta_{i=1,\ldots,N}=\theta_{\min},\ \varphi_{i=1,\ldots,N}=0} \approx \sum_{i=1}^{N} L_i \\ x_{\mathrm{P1E}} = x_{\mathrm{E}}\big|_{\theta_{\mathrm{E1}}=\theta_{\mathrm{E2}}=\theta_{\min},\ \varphi_{\mathrm{E1}}=\varphi_{\mathrm{E2}}=0} \approx 0 \\ z_{\mathrm{P1E}} = z_{\mathrm{E}}\big|_{\theta_{\mathrm{E1}}=\theta_{\mathrm{E2}}=\theta_{\min},\ \varphi_{\mathrm{E1}}=\varphi_{\mathrm{E2}}=0} \approx L_{\mathrm{E1}} + L_{\mathrm{E2}} \\ x_{\mathrm{P2T}} = -x_{\mathrm{P6T}} = \max(p_x) \\ z_{\mathrm{P2T}} = z_{\mathrm{P6T}} = p_z\big|_{p_x=\max(p_x)} \\ x_{\mathrm{P2E}} = -x_{\mathrm{P6E}} = \max(x_{\mathrm{E}}) \\ z_{\mathrm{P2E}} = z_{\mathrm{P6E}} = z_{\mathrm{E}}\big|_{x_{\mathrm{E}}=\max(x_{\mathrm{E}})} \\ x_{\mathrm{P3T}} = -x_{\mathrm{P5T}} = p_x\big|_{p_z=\min(p_z)} \\ z_{\mathrm{P3T}} = z_{\mathrm{P5T}} = \min(p_z) \\ x_{\mathrm{P3E}} = -x_{\mathrm{P5E}} = x_{\mathrm{E}}\big|_{Z_{\mathrm{E}}=\min(z_{\mathrm{E}})} \\ z_{\mathrm{P3E}} = z_{\mathrm{P5E}} = \min(z_{\mathrm{E}}) \\ x_{\mathrm{P4T}} = x_{\mathrm{P4E}} = p_x = 0 \\ z_{\mathrm{P4T}} = p_z\big|_{p_x=0} \\ z_{\mathrm{P4E}} = z_{\mathrm{E}}\big|_{x_{\mathrm{E}}=0} \end{cases} \tag{9}$$

E. Workspace area and volume calculation algorithm

Once the boundary shape is obtained by using the ETS method (e.g. the blue line in Fig. 4), the workspace area can be calculated (e.g. using the Convhull function in Matlab). Then, the workspace volume can be calculated by rotating the workspace area around the z-axis. Fig. 5 shows the example boundary lines and a quarter of the workspace volume generated by the exhaustive approach and the ETS method. The pseudocode of the ETS method is shown in **Algorithm 2**.

Algorithm 2: Workspace calculation by the ETS method

Inputs: Sampling interval value D; Number of segments N; Maximum bending angle $\theta_{\max}$; Section length L;
Outputs: Workspace area (A) and volume (V)
Algorithm:
$[L_{\mathrm{E1}}, L_{\mathrm{E2}}, \theta_{\mathrm{E1max}}, \theta_{\mathrm{E2max}}] \leftarrow f\{D, N, \theta_{\max}, L\}$ ▷Calculate ETS parameters
$\boldsymbol{\theta}_{\mathrm{E1}} \leftarrow \{[\theta_{\min}, 1, 2, \ldots, \theta_{\mathrm{E1max}}]*\cos(0); [\theta_{\min}, 1, 2, \ldots, \theta_{\mathrm{E1max}}]*\cos(\pi)\}$
$\boldsymbol{\theta}_{\mathrm{E2}} \leftarrow \{[\theta_{\min}, 1, 2, \ldots, \theta_{\mathrm{E2max}}]*\cos(0); [\theta_{\min}, 1, 2, \ldots, \theta_{\mathrm{E2max}}]*\cos(\pi)\}$
▷Generate the bending angle matrix
for $i \leftarrow 1$ to **size**($\boldsymbol{\theta}_{\mathrm{E1}}$) **do**
  $\theta_1 \leftarrow \boldsymbol{\theta}_{\mathrm{E1}}(i)$
  for $j \leftarrow 1$ to **size**($\boldsymbol{\theta}_{\mathrm{E2}}$) **do**
    $\theta_2 \leftarrow \boldsymbol{\theta}_{\mathrm{E2}}(j)$
    $[{}^0\boldsymbol{T}_1, {}^1\boldsymbol{T}_2] \leftarrow f\{L_{\mathrm{E1}}, L_{\mathrm{E2}}, \theta_{\mathrm{E1max}}, \theta_{\mathrm{E2max}}\}$ ▷Calculate the HTM, Eq.(1)
    ${}^0\boldsymbol{T}_2 \leftarrow {}^0\boldsymbol{T}_1 * {}^1\boldsymbol{T}_2$
    $\boldsymbol{P}[x, z] \leftarrow f\{{}^0\boldsymbol{T}_2\}$ ▷Calculate the distal position matrix, Eq.(4)
  end for
end for
[BL, A] ← *find the boundary line* (BL) *and area* (A) *of* $\boldsymbol{P}[x, z]$
BS ← *rotate* BL *to generate the boundary surface* (BS)
V ← *calculate the volume of* BS
return A, V

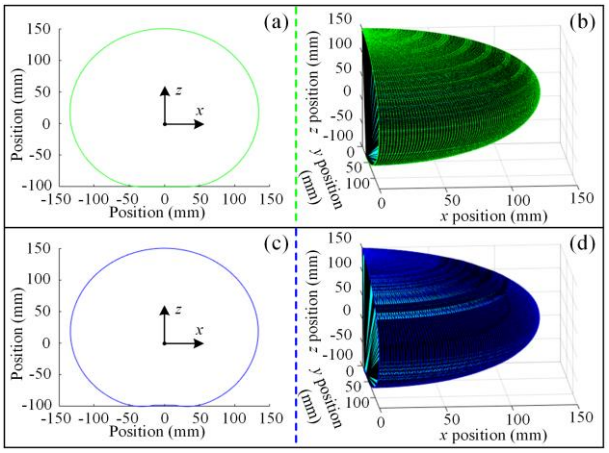

Fig. 5. Example boundary lines and boundary surfaces with N=3, D=1°, L=50mm, $\theta_{\max}$=180°. (a) Boundary line of the true workspace (Algorithm 1). (b) A quarter of the boundary surface of the true workspace (Algorithm 1). (c) Boundary line from the ETS method (Algorithm 2). (d) A quarter of the boundary surface from the ETS method (Algorithm 2).

III. SIMULATION EXPERIMENTS AND RESULTS

A. Simulation environment

All simulations are run on MATLAB R2020a software in a high-performance computing cluster, and its configurations are Intel(R) Xeon(R) Gold 6238R CPU @ 2.20GHz processors, 18GB System memory, and Quadro RTX 5000 GPU. Considering the computation time and memory consumption of the exhaustive approach (Algorithm 1), the maximum sample number of the distal point positions is set as 10^8. The interval of bending angle (D) is chosen as 1° if the total sample number is less than or equal to 10^8. With the increase of the number of segments of a continuum robot, if the total sample number is greater than 10^8, the interval of bending angle (D) is increased to limit the total sample distal point positions to less than 10^8.

B. Workspace analysis

The workspace of a continuum robot is determined mainly by the length of segments (L), the maximum bending angle ($\theta_{\max}$) of each segment and the number of segments (N). Fig. 6 shows the results of workspace analyses with various maximum bending angles ($\theta_{\max}$) and different number of segments (N). It can be seen that, for a continuum robot with the number of segments (N) less than a certain threshold, its workspace is not a fully complete (or filled) area in 2D or volume in 3D (Fig. 6(a)-(e)). The maximum bending angle ($\theta_{\max}$) of each segment has effects on the workspace as well. When the number of segments and the bending angle reaches a certain threshold, the workspace becomes a complete or fully filled area or volume (Fig. 6(f)-(j)). Table II and Table III show the configurations of a continuum robot with incomplete (marked with ★) and complete workspace area (in 2D) and volume (in 3D), respectively.

For a continuum robot with incomplete workspaces (e.g. Fig.6 (a)-(e)), the exhaustive approach can be used to estimate its workspace. The computational cost can be handled in this case because both the number of segments (N) and the maximum bending angle ($\theta_{\max}$) are small. Attentions need to be paid to the selection of the interval of bending angle (D)

when generating the sample distal positions. When the number of segments (N) of a robot is increased to a certain threshold, the workspace becomes complete. The exhaustive approach is hardly used due to computational cost. Then the ETS method can be utilized for workspace calculation.

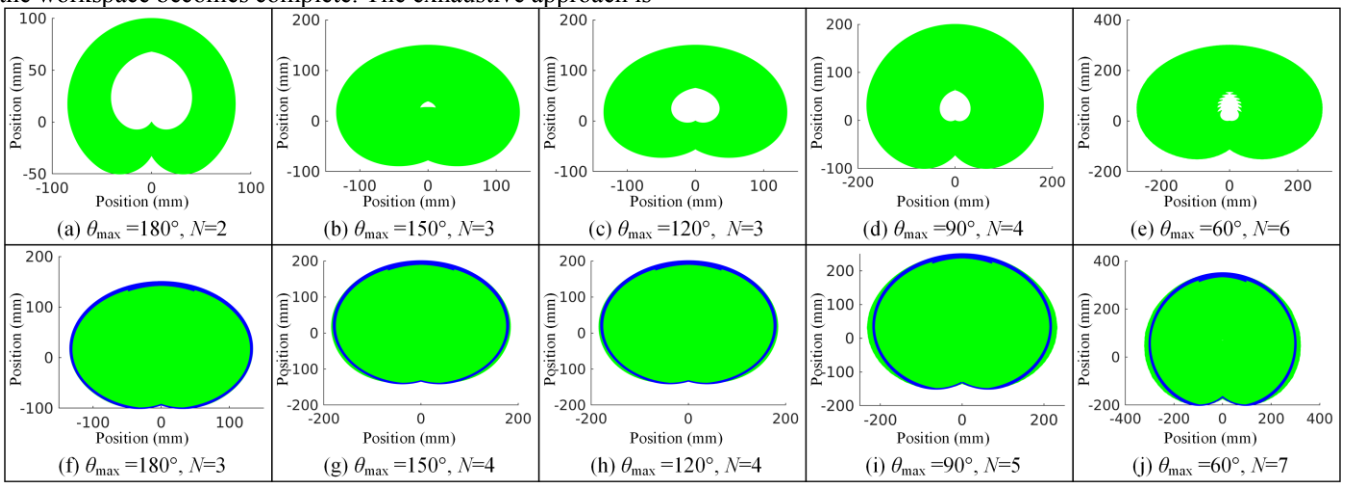

Fig. 6. Workspace with different parameters. The green color shows the true workspace area, and the blue lines show the boundary calculated by the ETS method.

TABLE II
SUMMARY OF WORKSPACE AREA CALCULATED BY THE ETS METHOD

θ_{max}	N	2	3	4	5	6	7	8
30°	True (mm^2)	2.31E+02	1.89E+03	7.81E+03	2.22E+04	5.19E+04	1.03E+05	1.78E+05
60°	True (mm^2)	1.20E+03	1.09E+04	4.24E+04	1.04E+05	1.91E+05	2.83E+05	3.83E+05
	ETS (mm^2)	★	★	★	★	★	2.67E+05	3.67E+05
	ETS error (%)	★	★	★	★	★	-5.58	-4.35
90°	True (mm^2)	3.39E+03	2.76E+04	8.34E+04	1.47E+05	2.20E+05	3.12E+05	4.15E+05
	ETS (mm^2)	★	★	★	1.40E+05	2.14E+05	3.04E+05	4.09E+05
	ETS error (%)	★	★	★	-4.83	-2.76	-2.77	-1.49
120°	True (mm^2)	6.85E+03	4.42E+04	9.50E+04	1.57E+05	2.34E+05	3.25E+05	4.30E+05
	ETS (mm^2)	★	★	9.17E+04	1.53E+05	2.30E+05	3.23E+05	4.31E+05
	ETS error (%)	★	★	-3.49	-2.73	-1.73	-0.80	0.28
150°	True (mm^2)	1.12E+04	5.15E+04	1.01E+05	1.65E+05	2.44E+05	3.36E+05	4.41E+05
	ETS (mm^2)	★	★	9.80E+04	1.61E+05	2.40E+05	3.34E+05	4.44E+05
	ETS error (%)	★	★	-2.77	-2.25	-1.56	-0.36	0.81
180°	True (mm^2)	1.55E+04	5.35E+04	1.02E+05	1.65E+05	2.44E+05	3.37E+05	4.41E+05
	ETS (mm^2)	★	5.35E+04	1.02E+05	1.67E+05	2.47E+05	3.42E+05	4.54E+05
	ETS error (%)	★	-0.03	0.14	0.91	1.08	1.48	2.94

★ shows that the workspace is incomplete, in which case an exhaustive approach is suggested for use in calculating the workspace.

C. *Workspace area*

Before analyzing the workspace volume calculated by the ETS method, this section analyses the workspace in 2D, which is defined as the maximum cross-sectional area of the workspace volume (named workspace area). For comparison, true workspace estimated by the exhaustive approach (**Algorithm 1**) is used in the analyses.

Table II shows the results of the workspace area calculated by the ETS method for a continuum robot with various combinations of the number of segments (N) and the maximum bending angle (θ_{max}). The length of each segment is assumed to be 50mm in the simulation. The results show that the maximum and minimum errors of workspace area calculated by the ETS method, compared to the true workspace area estimated by the exhaustive approach, are -5.58% and -0.03% when N=7, θ_{max}=60° and N=3, θ_{max}=180°, respectively. When N=3 and θ_{max}=180°, the workspace from the ETS model has almost the same as the true workspace, hence it has the minimum error. With the increase of N and θ_{max}, the error decreases. However, once these two parameters are over a certain threshold (e.g. N >7 and θ_{max}=120°/150°; N >4 and θ_{max}=180°), the errors will become a positive value (i.e. the workspace from the ETS method is greater than that of the exhaustive approach), which proves that the ETS method has better performance and more close to the real true workspace than the exhaustive approach when the computational resource is limited.

D. *Workspace volume*

Table III shows the results of workspace volume calculated by the ETS method for a continuum robot with various combinations of the number of segments (N) and the maximum bending angle (θ_{max}). The length of each segment is assumed to be 50mm. The true workspace volumes calculated by the exhaustive approach (**Algorithm 1**) are included for comparison. The results show that the maximum and minimum errors of workspace volume estimated by the ETS

method compared to the true workspace volume calculated by the exhaustive approach are -12.33% and -1.62% when N=7, θ_{max}=60° and N=8, θ_{max}=180°, respectively. Similar to the workspace area results, with the increase of N and θ_{max}, the errors are decreased.

Additionally, the ETS method has a significantly better performance when considering computational efficiency. Although the maximum sample number of the exhaustive approach is settled as 10^8, its computation time still expands with the increase of N and θ_{max}. In contrast, the robot configurations have no effect on the computational cost of the ETS method, and the ETS method takes almost the same time of 2s for all the configurations. For example, the efficiency of the ETS method is 196 times better than the exhaustive approach when N=8 and θ_{max}=150°. The reason we compare the ETS method with an exhaustive approach is that the exhaustive approach has an adequate efficiency among numerical methods, and other methods, e.g. improved Monte Carlo method [25] [27], can hardly be applied to a continuum robot with multi-segment.

TABLE III
SUMMARY OF WORKSPACE VOLUME CALCULATED BY THE ETS METHOD

θ_{max}	N	2	3	4	5	6	7	8
30°	True (mm^3)	1.07E+04	2.17E+05	1.46E+06	5.74E+06	1.63E+07	3.60E+07	6.94E+07
	t_{True} (s)	1	1	6	80	92	188	293
60°	True (mm^3)	1.42E+05	2.32E+06	1.18E+07	3.33E+07	6.86E+07	1.22E+08	1.92E+08
	t_{True} (s)	1	2	67	86	121	183	315
	ETS (mm^3)	★	★	★	★	★	1.07E+08	1.70E+08
	ETS error (%)	★	★	★	★	★	**-12.33**	-11.36
90°	True (mm^3)	5.33E+05	6.10E+06	2.09E+07	4.60E+07	8.59E+07	1.43E+08	2.23E+08
	t_{True} (s)	1	3	40	85	120	280	355
	ETS (mm^3)	★	★	★	4.05E+07	7.61E+07	1.28E+08	1.98E+08
	ETS error (%)	★	★	★	-11.95	-11.47	-10.95	-11.22
120°	True (mm^3)	1.12E+06	8.59E+06	2.35E+07	5.04E+07	9.26E+07	1.53E+08	2.35E+08
	t_{True} (s)	2	6	41	72	120	216	266
	ETS (mm^3)	★	★	2.14E+07	4.55E+07	8.35E+07	1.38E+08	2.13E+08
	ETS error (%)	★	★	-9.10	-9.64	-9.91	-9.41	-9.50
150°	True (mm^3)	1.70E+06	9.43E+06	2.52E+07	5.20E+07	9.30E+07	1.48E+08	2.29E+08
	t_{True} (s)	2	11	38	74	197	186	**393**
	ETS (mm^3)	★	★	2.34E+07	4.90E+07	8.80E+07	1.43E+08	2.21E+08
	ETS error (%)	★	★	-6.91	-5.81	-5.43	-3.40	-3.37
180°	True (mm^3)	2.08E+06	9.77E+06	2.55E+07	5.26E+07	9.32E+07	1.51E+08	2.31E+08
	t_{True} (s)	2	17	39	76	153	200	343
	ETS (mm^3)	★	9.45E+06	2.48E+07	5.13E+07	9.15E+07	1.49E+08	2.27E+08
	ETS error (%)	★	-3.27	-2.88	-2.31	-1.84	-1.70	**-1.62**

★ shows that the workspace is incomplete, in which case an exhaustive approach is suggested for use in calculating the workspace.

IV. DISCUSSION

This research proposed an ETS method for calculating the workspace of multi-segment continuum robots. The results show that the ETS method is efficient and accurate enough for workspace calculation. The accuracy increases with an increase in the number of segments (N) and the maximum being angle (θ_{max}). When applying the ETS method, the robot parameters need to be compared with a certain threshold, which is suggested by Tables II and III. However, because of the complex internal cavity of the workspace, the current ETS method is limited in several cases (marked with ★in Table II and Table III). Therefore, further investigation can be conducted to determine the internal cavity and improve the accuracy of the threshold of the proposed ETS method.

In this research, all the segments are assumed to be identical. For a continuum robot that has different lengths or different bending angles among its segments, this ETS method needs to be modified, which is also one of the future research tasks.

Additionally, this paper does not consider the diameter of a continuum robot when applying general kinematics to calculate its distal point position. Self-collision among segments needs to be considered when calculating accurate workspace or controlling the motion of robots.

V. CONCLUSION

An Equivalent Two Sections (ETS) method based on the forward kinematic and piecewise constant curvature (PCC) model was proposed in this paper. It is a numerical method for the estimation of the workspace of a continuum robot with many segments. Extensive simulations with six different maximum bending angles (θ_{max}) and seven different number of segments (N) were conducted and verified the efficiency and accuracy of the ETS method. By comparing to the true workspace calculated by an exhaustive approach, the ETS method was demonstrated to be very efficient and accurate enough.

REFERENCES

[1] S. Kolachalama, and S. Lakshmanan, "Continuum robots for manipulation applications: A survey," *Journal of Robotics,* vol. 2020, pp. 1-19, Jul. 2020.

[2] J. Burgner-Kahrs, D. C. Rucker, and H. Choset, "Continuum robots for medical applications: A survey," *IEEE Transactions on Robotics,* vol. 31, no. 6, pp. 1261-1280, Dec. 2015.

[3] M. Wang, X. Dong, W. Ba, A. Mohammad, D. Axinte, and A. Norton, "Design, modelling and validation of a novel extra slender continuum robot for in-situ inspection and repair in aeroengine," *Robotics and Computer-Integrated Manufacturing,* vol. 67, pp. 1-11, Feb. 2021.

[4] A. Mehrkish, and F. Janabi-Sharifi, "A comprehensive grasp taxonomy of continuum robots," *Robotics and Autonomous Systems*, vol. 145, pp. 103860, Nov. 2021.

[5] H. Wang, Z. Chen, and S. Zuo, "Flexible manipulator with low-melting-point alloy actuation and variable stiffness," *Soft Robotics*, vol. 9, no. 3, pp. 577-590, Jun. 2021.

[6] B. Lin, J. Wang, S. Song, B. Li, and M. Q.-H. Meng, "A modular lockable mechanism for tendon-driven robots: design, modeling and characterization," *IEEE Robotics and Automation Letters*, vol. 7, no. 2, pp. 2023-2030, Apr. 2022.

[7] Y. J. Kim, S. Cheng, S. Kim, and K. Iagnemma, "A novel layer jamming mechanism with tunable stiffness capability for minimally invasive surgery," *IEEE Transactions on Robotics,* vol. 29, no. 4, pp. 1031-1042, Aug. 2013.

[8] Y. Kim, S. S. Cheng, and J. P. Desai, "Active stiffness tuning of a spring based continuum robot for MRI-guided neurosurgery," *IEEE Transactions on Robotics,* vol. 34, no. 1, pp. 18-28, Feb. 2018.

[9] Z. Xing, F. Wang, Y. Ji, D. McCoul, X. Wang, and J. Zhao, "A structure for fast stiffness-variation and omnidirectional-steering continuum manipulator," *IEEE Robotics and Automation Letter,* vol. 6, no. 2, pp. 755-762, Apr. 2021.

[10] C. Carlo, A. Pistone, D. Ludovico, P. Guardiani, R. Gagliardi, L. D. M. C. D. Verme, G. Sofia, and D. G. Caldwell, "Design of a novel long-reach cable-driven hyper-redundant snake-like manipulator for inspection and maintenance," *Applied Sciences*, vol. 12, no. 7, pp. 3348, Mar. 2022.

[11] G. Qin, A. Ji, Y. Cheng, W. Zhao, H. Pan, S. Shi, and Y. Song, "A snake-inspired layer-driven continuum robot," *Soft Robotics*, vol. 9, no. 4, pp. 788-797, Aug. 2022.

[12] Y. Gao, K. Takagi, T. Kato, N. Shono and N. Hata, "Continuum robot with follow-the-leader motion for endoscopic third ventriculostomy and tumor biopsy," *IEEE Transactions on Biomedical Engineering*, vol. 67, no. 2, pp. 379-390, Feb. 2020.

[13] M. Nan, S. Monk, and D. Cheneler, "Modelling and analysis of the spital branched flexure-hinge adjustable-stiffness continuum robot," *Robotics*, vol. 11, no. 5, pp. 97, Sep. 2022.

[14] W. R. Wockenfuß, V. Brandt, L. Weisheit and W. G. Drossel, "Design, modeling and validation of a tendon-driven soft continuum robot for planar motion based on variable stiffness structures," *IEEE Robotics and Automation Letters*, vol. 7, no. 2, pp. 3985-3991, Apr. 2022.

[15] X. Jing, J. Jiang, F. Xie, C. Zhang, S. Chen and L. Yang, "Continuum manipulator with rigid-flexible coupling structure," *IEEE Robotics and Automation Letters*, vol. 7, no. 4, pp. 11386-11393, Oct. 2022.

[16] J. Fathi, T. J. C. Oude Vrielink, M. S. Runciman and G. P. Mylonas, "A deployable soft robotic arm with stiffness modulation for assistive living applications," in *2019 International Conference on Robotics and Automation (ICRA)*, pp. 1479-1485, May. 2019.

[17] I. D. Falco, M. Cianchetti, and A. Menciassi, "A soft multi-module manipulator with variable stiffness for minimally invasive surgery" *Bioinspiration & Biomimetics*, Vol. 12, no. 5, pp. 056008, Sep. 2017.

[18] Y. Fan, D. Liu and L. Ye, "A novel continuum robot with stiffness variation capability using layer jamming: design, modeling, and validation," *IEEE Access*, vol. 10, pp. 130253-130263, Dec. 2022.

[19] Y. Zhu, B. Jin, W. Li, and S. Li, "Optimal design of hexapod walking robot leg structure based on energy consumption and workspace," *Transactions of the Canadian Society for Mechanical Engineering,* vol. 38, no. 3, pp. 305-317, Sep. 2014.

[20] M. A. Hosseini, and H. M. Daniali, "Cartesian workspace optimization of tricept parallel manipulator with machining application," *Robotica*, vol. 33, no. 9, pp. 1948-1957, 2015

[21] B. He, S. Hou, Z. Deng, J. Cao, and W Liu, "Workspace analysis of a novel underactuated robot wrist based on equivalent prototyping," *The International Journal of Advanced Manufacturing Technology,* vol. 72, no. 1, pp. 531-541, 2014.

[22] K. Abdel-Malek, H. J. Yeh, and S. Othman, "Interior and exterior boundaries to the workspace of mechanical manipulators," *Robotics and Computer Integrated Manufacturing*, vol. 16, pp. 365-376, 2000.

[23] J. Burgner-Kahrs, H. B. Gilbert, J. Granna, P. J. Swaney and R. J. Webster, "Workspace characterization for concentric tube continuum robots," in *Proceedings of the 2014 IEEE/RSJ International Conference on Intelligent Robots and Systems*, pp. 1269-1275, 2014.

[24] Y. Cao, K. Lu, X. Li, and Y. Zang, "Accurate numerical methods for computing 2D and 3D robot workspace," *International Journal of Advanced Robotic Systems*, vol. 8, no. 6, pp. 1-13. 2011.

[25] B. He, X. Zhu, and D. Zhang, "Boundary encryption-based Monte Carlo learning method for workspace modeling," *Journal of Computing and Information Science in Engineering,* vol. 20, no. 3, 2020.

[26] Y. Zhou, J. Niu, Z. Liu, and F. Zhang, "A novel numerical approach for workspace determination of parallel mechanisms," *Journal of Mechanical Science and Technology*, vol. 31, no. 6, pp. 3005-3015, 2017.

[27] A. Peidró, O. Reinoso, A. Gil, J. M. Marín, and L. Payá, "An improved Monte Carlo method based on Gaussian Growth to calculate the workspace of robots," *Engineering Applications of Artificial Intelligence*, vol. 64, pp. 197-207, 2017.

[28] Y. Gao, K. Takagi, T. Kato, N. Shono and N. Hata, "Continuum robot with follow-the-leader motion for endoscopic third ventriculostomy and tumor biopsy," *IEEE Transactions on Biomedical Engineering*, vol. 67, no. 2, pp. 379-390, Feb. 2020.

[29] B. A. Jones, and I. D. Walker, "Kinematics for multisection continuum robots," *IEEE Transactions on Robotics*, vol. 22, no. 1, pp. 43-55, 2006.

[30] C. Della Santina, A. Bicchi and D. Rus, "On an improved state parametrization for soft robots with piecewise constant curvature and its use in model based control," *IEEE Robotics and Automation Letters*, vol. 5, no. 2, pp. 1001-1008, Apr. 2020.

[31] T. George Thuruthel, Y. Ansari, E. Falotico, and C. Laschi, "Control strategies for soft robotic manipulators: A survey," *Soft Robotics,* vol. 5, no. 2, pp. 149-163, Apr. 2018.